Articles

Catalytic Protein Film Voltammetry from a Respiratory Nitrate Reductase Provides Evidence for Complex Electrochemical Modulation of Enzyme Activity†

Lee J. Anderson,‡ David J. Richardson,§ and Julea N. Butt*,‡

School of Chemical Sciences and School of Biological Sciences, Centre for Metalloprotein Spectroscopy and Biology, University of East Anglia, Norwich NR4 7TJ, U.K.

Received November 28, 2000; Revised Manuscript Received June 15, 2001

ABSTRACT: The first step in the respiratory reduction of nitrate to dinitrogen in *Paracoccus pantotrophus* is catalyzed by the quinol-nitrate oxidoreductase NarGHI. This membrane-anchored protein directs electrons from quinol oxidation at the membrane anchor, NarI, to the site of nitrate reduction in the membrane extrinsic [Fe-S] cluster and Mo-bis-MGD containing dimer, NarGH. Liberated from the membrane, NarGH retains its nitrate reductase activity and forms films on graphite and gold electrodes within which direct and facile exchange of electrons between the electrode and the enzyme occurs. Protein film voltammetry has been used to define the catalytic behavior of NarGH in the potential domain and a complex pattern of reversible, nitrate concentration dependent modulation of activity has been resolved. At low nitrate concentrations the local maximum observed in the catalytic current−potential profile reveals how NarGH can catalyze nitrate reduction via two pathways having distinct specificity constants, k_{cat}^{obs}/K_M^{obs}. Catalysis is directed to occur via one of the pathways by an electrochemical event within NarGH. On increasing the nitrate concentration, the local maximum in the catalytic current becomes less distinct, and the catalytic waveform adopts an increasingly sigmoidal form. A pattern of voltammetry similar to that observed during nitrate reduction is observed during reduction of the stereochemically distinct substrate chlorate. Centers whose change of oxidation state may define the novel catalytic voltammetry of NarGH have been identified by EPR-monitored potentiometric titrations and mechanisms by which the electrochemistry of Mo-bis-MGD or [Fe-S] clusters can account for the observed behavior are discussed.

The ability to utilize nitrate as a respiratory substrate is widespread in bacteria where several biochemically distinct nitrate reductases have been identified (*1*, *2*). The soil bacterium *Paracoccus pantotrophus*[2] expresses two respiratory nitrate reductases, NapAB and NarGHI.[1] These enzymes are distinguished by their cellular location, their subunit composition, and the number and identity of their redox centers, but both contain a Mo-bis-molybdopterin guanine dinucleotide (Mo-bis-MGD) center catalyzing the reduction of nitrate to nitrite:

$$NO_3^- + 2e^- + 2H^+ \rightarrow NO_2^- + H_2O$$

NapAB exemplifies the soluble periplasmic respiratory nitrate reductases with two c-type hemes, an [Fe-S] cluster and Mo-bis-MGD coordinated by a dimeric protein (*3*−*5*). Predominantly expressed under aerobic conditions, NapAB receives its electrons from the quinol pool via the membrane-anchored protein NapC and dissipates the free energy of the QH_2/NO_3^- couple (*1*, *6*). By contrast, the quinol-nitrate oxidoreductase, NarGHI, expressed during anaerobic growth is anchored to the membrane and conserves the free energy of the QH_2/NO_3^- couple as a transmembrane electrochemical proton gradient in the first step of the denitrification pathway (*2*, *7*, *8*). NarGHI has a wide distribution being found not only in the denitrifying bacteria but also in many enteric bacteria including *Escherichia coli* (*9*−*11*) and shares extensive sequence homology with a large family of membrane-associated [Fe-S] cluster and molybdenum-containing enzymes (*2*). Examples include *E. coli* DMSO reductase (DmsABC), *Wolinella succinogenes* formate dehydrogenase (FdhABC), *W. succinogenes* polysulfide reductase (PsrABC), and *Salmonella typhimurium* tetrathionate reductase (TtrABC) (*12*).

NarGHI catalyzes quinol oxidation at the periplasmic face of the diheme containing membrane anchor NarI (25 kDa), as in Figure 1 (*11*, *13*). Protons are released into the periplasm while electrons are directed toward the cytoplasmically facing membrane extrinsic dimer, NarGH, where

† This work was funded by The Wellcome Trust, Grant 050709.

* Corresponding author tel: 44 1603 593877; fax: 44 1603 592003; e-mail: j.butt@uea.ac.uk.

‡ School of Chemical Sciences.

§ School of Biological Sciences.

[1] Abbreviations: EPR, electron paramagnetic resonance; MGD, molybdopterin guanine dinucleotide; NapAB, periplasmic nitrate reductase; NarGH, membrane extrinsic dimer of NarGHI; NarGHI, membrane-anchored quinol-nitrate oxidoreductase; PGE, pyrolytic graphite edge; QH_2, membrane-associated quinol; SDS−PAGE, sodium dodecyl sulfate−polyacrylamide gel electrophoresis; SHE, standard hydrogen electrode.

[2] Formally known as *Thiosphaera pantotropha* and *Paracoccus denitrificans* GB17.

10.1021/bi002706b CCC: $20.00 © 2001 American Chemical Society
Published on Web 08/25/2001

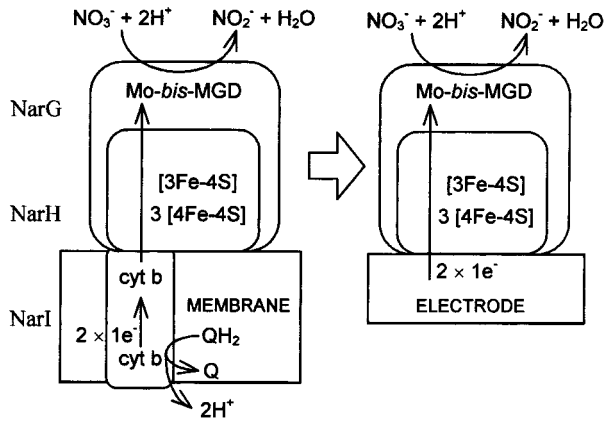

FIGURE 1: Cartoon of NarGHI in the cytoplasmic membrane of *P. pantotrophus* and NarGH receiving electrons directly from graphite and gold electrodes.

Scheme 1: Minimal Catalytic Cycle for Nitrate Reduction by a Mo-bis-MGD Enzyme

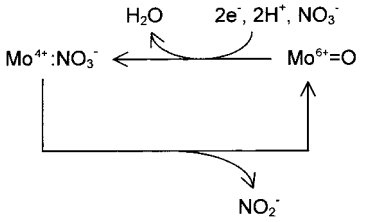

iron−sulfur clusters facilitate electron exchange between NarI and the site of nitrate reduction in NarG (*9*, *14*). NarH (61 kDa) contains one $[3Fe\text{-}4S]^{1+/0}$ and three $[4Fe\text{-}4S]^{2+/1+}$ clusters. The Mo-bis-MGD center and site of nitrate reduction are found in NarG (127 kDa). Up to four thiolate ligands from the MGD cofactors contribute to the coordination sphere of the Mo ion with additional ligands likely to be provided by a conserved serine residue and one or more nonprotein O ligands, which can include oxo, hydroxo, or water (*1*, *15*, *16*). Changes in the number and protonation state of the Mo ion's nonprotein O ligands as the metal switches oxidation state are likely to be mechanistically important as an oxygen atom is exchanged between nitrate and water via the Mo ion as it cycles between its 6+ and 4+ oxidation states, as in Scheme 1 (*17*).

Extensive spectroscopic characterization of NarGH(I) is limited to the enzyme from *E. coli*. EPR spectroscopy has identified multiple spectra originating from Mo^{5+}, which indicate a flexibility of coordination environment for the molybdenum ion in this oxidation state (*18*−*20*). A similar situation is found in many Mo-bis-MGD enzymes with the possibility that each Mo oxidation state exists in multiple coordination geometries (*5*, *17*, *21*). The Mo^{5+} EPR signals from NarGHI exhibit a transition between "low pH" and "high pH" forms (*10*, *18*−*20*). Equilibrium titrations of *E. coli* NarGHI at pH 8.1 show that the high pH signal titrates with $E_{m,8.1}(Mo^{5+/4+}) = +90$ mV and $E_{m,8.1}(Mo^{6+/5+}) = +250$ mV, while the low pH signal titrates with $E_{m,5.9}(Mo^{5+/4+}) = +200$ mV but resists oxidation at potentials up to +400 mV (*10*). Changes in the low pH signal observed when nitrate, nitrite, and the alternative substrate chlorate are added to the enzyme suggest that these anions bind in the vicinity of Mo^{5+} in this enzyme form (*15*, *19*). Although the functional significance of these observations is not yet clear, the decrease in nitrate reductase activity observed on raising the pH is reported to parallel the conversion from low to high pH forms of the enzyme (*10*, *18*). The hemes of NarGHI exhibit reduction potentials apparently well-poised to facilitate electron transfer from the quinol pool to the Mo-bis-MGD center and ultimately nitrate, $E_{m,7}$ (NO_3^-/NO_2^-) = +420 mV (*11*). The reduction potentials of the [Fe-S] clusters span from −420 to +180 mV in *E. coli NarGHI (10*, *22)*.

NarGH retains its nitrate reductase activity when liberated from the cytoplasmic membrane (*8*, *9*, *13*, *23*) and we have previously reported the spontaneous assembly of *P. pantotrophus* NarGH "films" on pyrolytic graphite edge (PGE) electrodes (*24*). Within these films the enzyme molecules retain their catalytic activity and are oriented for direct electron exchange with the electrode in a manner that may mimic their interaction with the membrane (Figure 1). Now with the redox centers of NarGH under the precise potential control of the electrode it is possible to map out variations in catalytic activity as these centers switch oxidation state in response to variation of the applied potential in a technique known as protein film voltammetry (*25*). The current flowing at each value of applied potential provides a measure of catalytic performance and is readily visualized through the current−potential profile obtained when the applied potential is swept linearly between two limits during cyclic voltammetry. In the absence of limitations from interfacial electron exchange or substrate delivery to the immobilized enzyme the catalytic response arising from an enzyme film is most informative. Under these conditions the position, steepness, and shape of the catalytic wave are determined by intrinsic thermodynamic and kinetic properties of the enzyme and its interaction with substrate (*26*); the catalytic waveform being defined by the reduction potentials of centers within NarGH together with rates for processes including intramolecular electron exchange, substrate binding, and product formation. We have previously demonstrated that such a situation exists when NarGH films catalyze nitrate reduction under steady-state conditions (*24*). The enzyme's influence over the reaction catalyzed is immediately revealed by the need to apply potentials below +100 mV at pH 6 and significantly below $E_m(NO_3^-/NO_2^-)$ to detect a catalytic reduction current. The steepness of the response under enzyme-limiting conditions suggested that a one-electron reduction step was important for progression through the catalytic cycle. However, there were indications that the response under nitrate-limiting conditions deviated from that predicted by consideration of simple catalytic cycles. We have now extended our initial investigations to include characterization of NarGH activity toward nitrate and chlorate reduction over a wide range of substrate concentration and pH. There is a striking dependence of the shape of the catalytic wave on substrate concentration.[3] At "high" substrate concentrations, resulting in enzyme-limited catalysis, a sigmoidal increase in catalytic current accompanies lowering of the applied potential. In contrast, under substrate-limiting conditions, the rate of catalysis is found to increase but then decrease on application of an increased driving force for the reduction. EPR-monitored potentiometric titrations have allowed us to

[3] While electrons, protons, nitrate, and chlorate are all substrates in the reactions catalyzed by NarGH, in this paper, the term substrate is used to refer only to nitrate or chlorate.

identify centers within *P. pantotrophus* NarGH whose change of oxidation state may contribute defining features to the voltammetric behavior of the enzyme, and mechanisms that account for the observed behavior are discussed.

EXPERIMENTAL PROCEDURES

Cell Growth and Membrane Isolation. P. pantotrophus (wild type) was grown in batch culture under anaerobic denitrifying conditions in minimal media with sodium acetate as the carbon source and nitrate as the terminal electron acceptor (*8*). Harvested cells were resuspended in 2 mM $MgCl_2$ and 100 mM Tris-HCl (pH 8, 4 °C) and broken using a continuous French press (70 psi). Cell debris was removed by 10 min of centrifugation at 12200*g*, and the supernatant was subjected to 4 h of ultracentrifugation at 48400*g* at 4 °C to pellet membrane vesicles. Membrane vesicles were resuspended in 2 mM $MgCl_2$ and 100 mM Tris-HCl (pH 8, 4 °C), frozen rapidly in liquid N_2, and stored at −80 °C.

Purification of NarGH. All procedures were performed at 4 °C. Membrane vesicles were thawed and diluted in 2 mM $MgCl_2$ and 100 mM Tris-HCl (pH 8.0) to give a total protein concentration of 15−20 mg mL^{-1}. Dodecylmaltoside (DDM) was added to a final concentration of 1.5% (m/v), and the solution was stirred for 60 min. Insoluble material was removed by 45 min of ultracentrifugation at 142200*g*, and the supernatant was applied to a DEAE Toyapearl column equilibrated with 0.05% DDM (m/v), 2 mM $MgCl_2$, 50 mM NaCl, and 100 mM Tris-HCl (pH 8.0). The loaded column was washed with two column volumes of the equilibration buffer, and a gradient of 50−500 mM NaCl was applied. Fractions containing maximal nitrate reductase activity eluted around 220 mM NaCl, were pooled, and then exchanged into 0.05% DDM (m/v) and 10 mM potassium phosphate (pH 7.0). UV−visible absorption spectroscopy showed b- and c-type hemes to be present. The sample was applied to a hydroxyapatite column equilibrated with 0.05% DDM (m/v) and 10 mM potassium phosphate (pH 7.0). Nitrate reductase activity (ca. 90% of that applied to the column) was recovered after washing the column with ca. 1 L of equilibration buffer. UV−visible absorption spectroscopy of the concentrated column wash material failed to detect the presence of b-type hemes, although a trace amount of c-type heme remained.

For protein film voltammetry, the trace amount of c-type heme remaining in the NarGH sample was removed by FPLC gel filtration on a S200 column (Pharmacia) with NarGH exchanged into 25 mM Hepes and 50 mM NaCl (pH 7.5). SDS−PAGE analysis of the NarGH sample after gel filtration showed bands of ca. 60 and 120 kDa in agreement with previous reports (*8*, *23*). Native PAGE analysis showed one band. Samples used for voltammetry had $A_{410}/A_{280} = 0.15 \pm 0.03$ and a specific activity of 8 μmol of nitrate consumed min^{-1} mg^{-1} at pH 6.0 and 30 °C. Gel filtration was also performed with Hepes replaced by Tris. The enzyme purified in a similar manner in each case, exhibited a comparable specific activity and indistinguishable protein film voltammetry. Purified NarGH was aliquoted and stored frozen in liquid N_2.

Enzyme Assays and Analytical Procedures. Nitrate reductase activity was measured spectrophotometrically by nitrate-dependent oxidation of reduced methyl viologen (ϵ_{600nm} = 13 700 M^{-1} cm^{-1}). To follow nitrate reductase activity during NarGH purification, assays were performed in an anaerobic cuvette containing 1 mM methyl viologen, 1 mM KNO_3, and 25 mM Mes (pH 6.0, 30 °C). Following the addition of aliquots of anaerobic dithionite solution to give a steady absorbance of 2 at 600 nm, the reaction was initiated by the addition of protein. Spectrophotometric assays to determine the pH dependence of NarGH activity were performed at 25 °C in the 5 mM buffer and 50 mM Na_2SO_4 solutions used during voltammetric studies and described below. Protein concentrations were estimated using bicinchoninic acid with bovine serum albumin as the standard.

EPR Spectroscopy and Potentiometric Titrations. Typically, 50% of NarGH activity was lost on removal of heme contaminants by gel filtration. Because of the large quantities of NarGH required for EPR-monitored potentiometric titrations, these were performed using protein from the hydroxyapatite column wash for which a full field sweep at 10 K showed the EPR spectrum to be dominated by signals from [Fe-S] clusters with minor resonances at $g \approx 6$ and 4.3, most likely due to a trace amount of high spin ferric heme and adventitious Fe(III), respectively. Redox titrations of NarGH in 25 mM Mes (pH 6.0) were performed by two methods in the presence of the following mediators (20 μM each): 2,3,5,6-tetramethyl-*p*-phenylendiamine, 2,6-dichlorophenol indophenol, phenazine methosulfate, methylene blue, indigo carmine, anthroquinone 2,6-sulfonate, anthroquinone 2-sulfonate, phenosafranine, safranine O, benzyl viologen, and methyl viologen. To ensure the stability of the low potential samples, it was found necessary to increase the methyl viologen and benzyl viologen concentration to 70 μM. All experiments were performed in an anaerobic chamber (N_2 atmosphere with O_2 content <2 ppm). Potentiostatically poised samples were prepared using a three-electrode cell configuration with an Autolab electrochemical analyzer controlled by GPES software (EcoChemie, Utrecht, NL). Sample aliquots (200 μL, anaerobic) were placed in a glassy carbon pot contained in an enclosed vessel thermostated at 2 °C, which served as the working electrode. Platinum counter and Ag/AgCl (saturated KCl) reference electrodes were housed in separate chambers contacting the protein sample via a Vycor Fritt and Luggin capillary, respectively. Samples were held at the desired potential with stirring until the current from the cell approached zero, the potential control of the sample was released, the sample potential was confirmed with the potentiostat operating in galvanostat mode, and the sample was rapidly removed from the cell, transferred to an EPR tube, and frozen. Chemically poised samples were prepared in an enclosed vessel thermostated at 2 °C by the addition of small aliquots of dithionite solutions to a stirring solution. EPR spectroscopy was performed on an X-band ER200-D spectrometer (Bruker Spectrospin) interfaced to an ESP1600 computer and fitted with a liquid helium flow cryostat (ESR-900; Oxford Instruments). Spin concentrations were calculated by integration of EPR absorption spectra by comparison to a Cu(II)−EDTA standard under nonsaturating conditions. The Mo^{5+} signal intensity was fitted to the following equation for two sequential one-electron transfers to a center

$$\text{signal intensity (\%)} = 1/(1 + \theta_1 + \theta_2^{-1}) \qquad (1)$$

where $\theta_i = \exp(41.9(E - E_i))$ and E_1 and E_2 are the reduction potentials for the addition of the first and second electrons, respectively.

Protein Film Voltammetry. PGE or polycrystalline gold working electrodes (3 mm diameter) were polished with an aqueous Al_2O_3 slurry, sonicated, rinsed with water, and dried with a tissue. NarGH films were prepared by "painting" a freshly polished working electrode with 1−2 μL of an ice cold solution containing 30−40 μM NarGH and 2 mM neomycin sulfate (Sigma) in either 25 mM Hepes and 50 mM NaCl (pH 7.5) or 25 mM Tris-HCl-50 mM NaCl (pH 7.5). After ca. 1 min, the excess protein solution was removed, and the electrode was placed in the electrochemical cell. The cell consisting of a Ag/AgCl (saturated KCl) reference electrode (25 °C) in a Luggin sidearm and a platinum wire counter electrode was thermostated at 25 °C and housed in an anaerobic chamber. Cyclic voltammetry was performed with an Autolab electrochemical analyzer using the analogue scan generator controlled by GPES software. Electrode rotation was with an EG&G model 636 rotator. Potentials are reported with reference to the SHE by addition of 0.197 V to those measured (*27*).

All buffer−electrolyte solutions into which the NarGH film was placed for electrochemical experiments included 2 mM neomycin sulfate to stabilize the protein film (*24*). Buffer−electrolyte solutions were brought to the desired pH by the addition of aliquots of 2 M NaOH or 2 M H_2SO_4. The influence of pH was investigated in solutions composed of 50 mM Na_2SO_4 and 5 mM of either acetic acid (pH 5−5.5), Mes (pH 5.5−6.7), Pipes (6.7−7.0), Hepes (pH 7.0−7.4), Epps (pH 7.4−8.6), Ches (8.6−10.0), Caps (pH 10.0−11.1), or a multicomponent buffer containing 10 mM each of acetic acid, Mes, Pipes, Epps, and Ches (pH 5.0−10.0). In control experiments, voltammetry at 4 and 500 μM nitrate was also performed at pH 6 with a buffer component of 10 mM citrate, 10 mM Pipes, or 5, 50, or 500 mM Mes and at pH 7.5 with 10 mM Tris, Hepes, or phosphate. Nitrate, nitrite, chlorate, and azide solutions of the desired concentration were prepared by dilution of 1 M KNO_3, 1 M KNO_2, 0.1 M $KClO_3$, or 0.1 M NaN_3 stock solutions prepared in 25 mM Mes and 50 mM Na_2SO_4 with the pH confirmed to be 6. All reagents were of Analar quality or higher, and all solutions for voltammetry were prepared in water with total N and total Cl <0.1 ppm (Fisher).

A number of experimental approaches were taken to quantitate the variation of catalytic current magnitude at a given potential (i^E_{cat}) with substrate concentration, substrate identity, or pH. In each case, the response of the film in the condition of interest was normalized to that obtained in a standard solution to account for film to film variation of i^E_{cat}. In the first method, three voltammograms from a freshly prepared film were recorded in the solution of interest, and the film was transferred to a standard solution where further voltammograms were obtained. The current magnitude of the third scan in the solution of interest was then normalized against that of the second scan in the standard solution. i^E_{cat} was determined as the difference between the measured current and the noncatalytic current at potential E; the latter estimated by linear extrapolation of the noncatalytic part of the voltammogram. The validity of this approach to approximating the noncatalytic current was confirmed when

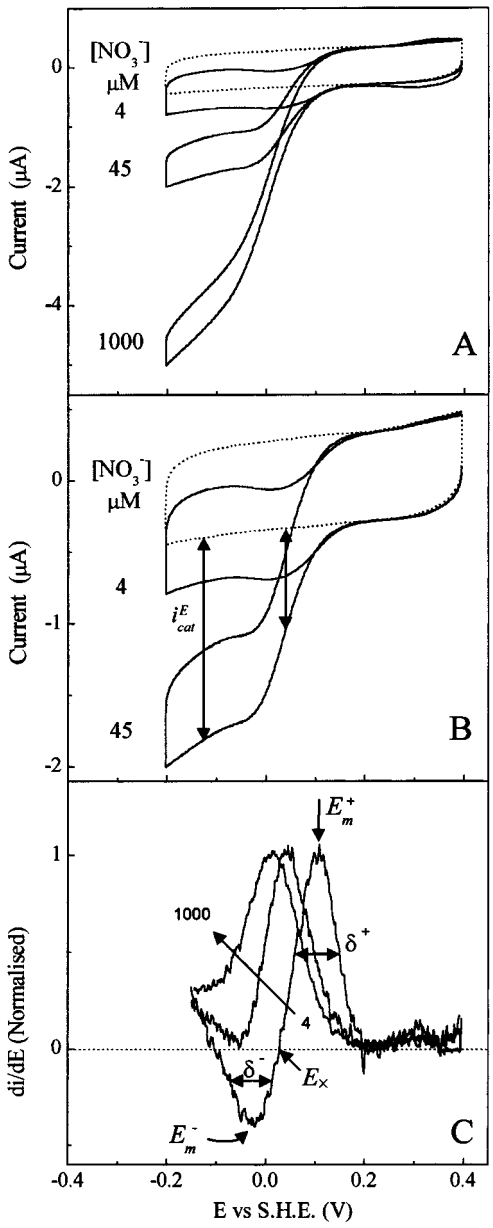

FIGURE 2: Influence of nitrate concentration on the voltammetric response arising from *P. pantotrophus* NarGH films prepared on a PGE electrode. (A) Cyclic voltammograms recorded in 4, 45, and 1000 μM nitrate. (B) Expanded view of the voltammograms at 4 and 45 μM nitrate. The broken lines illustrate the response obtained after addition of 100 μM azide to the 45 μM nitrate response. (C) Plot of the first derivative of the catalytic current with respect to applied potential for each catalytic voltammogram shown in panel A; the diagonal arrow indicates the direction of increasing nitrate concentration. For clarity, the magnitude of the positive feature in each derivative has been normalized. In panel B, the vertical lines at −130 and 30 mV illustrate measurement of i^E_{cat} for the response at 45 μM nitrate. In panel C, the parameters E^+_m, E^-_m, $E_\times$, δ^+, and δ^- are indicated for the 4 μM nitrate response. NarGH films were prepared as described in the Experimental Procedures. Voltammograms were recorded with a scan rate of 10 mV s^{-1} and electrode rotation at 3000 rpm in buffer−electrolyte solution of 2 mM neomycin, 25 mM Mes, and 50 mM Na_2SO_4, pH 6, at 25 °C.

the catalytic response from NarGH-coated electrodes was inhibited by azide (see, for example, Figure 2) in experiments that provided a further measure of i^E_{cat}. An alternative measure of the variation of i^E_{cat} with nitrate and chlorate concentration was provided when a NarGH-coated electrode

was placed in buffer−electrolyte solution, poised at the desired potential, and rotated at 3000 rpm, and the current was measured as substrate was titrated into the cell. Constant current readings were obtained within 10 s of the addition of an aliquot of substrate to the cell. Variation of i_{cat}^{E} with nitrate and chlorate concentration, C_s, was analyzed by fitting to a Michaelis−Menten expression of the form

$$i_{cat}^{E} = (i_{max}^{E} C_s)/(C_s + K_M^{obs}(E)) \quad (2)$$

to obtain values for the experimentally determined Michaelis constant, $K_M^{obs}(E)$, and maximum current, i_{max}^{E}. Results obtained from the various experimental approaches employed were indistinguishable. While performing detailed characterization of the shape of the voltammetric response at 4 μM nitrate it became desirable to change the pH in situ. Following voltammetry at a given pH, aliquots of typically 2−5 μL of 5 M H_2SO_4 or 5 M NaOH were added directly into the stirring electrochemical cell, voltammetry was recorded, and the pH of the cell solution was determined. The 4 and 45 μM nitrate catalytic current derivatives plotted in Figure 2 were obtained after averaging 16 consecutive voltammograms in the solution of interest to minimize signal-to-noise. Close scrutiny of the di/dE plots obtained in this way showed that there was no deviation from the derivative of each individual scan.

RESULTS

Steady-State Catalytic Voltammetry from NarGH Film at pH 6. Cyclic voltammograms from an enzyme film catalyzing substrate reduction reflect steady-state behavior when the current−potential profiles of the forward and reverse voltammetric sweeps superimpose after baseline subtraction. NarGH films prepared on PGE electrodes and placed into solutions of nitrate exhibit steady-state voltammograms when the electrode is rotated at 3000 rpm and cyclic voltammetry is performed with a scan rate of 10 mV s^{-1} (*24*). Typical catalytic voltammograms from a NarGH film measured under these conditions in 4, 45, and 1000 μM nitrate are illustrated in Figure 2A. It is immediately apparent that the magnitude of the catalytic response increases with each increase in nitrate concentration. Most interestingly, and highlighted by the expanded 4 and 45 μM nitrate responses of Figure 2B, each catalytic response also exhibits a unique shape. At 4 μM nitrate, the catalytic current exhibits a local maximum at +7 mV in both the forward and the reverse potential sweeps. By contrast, the responses in 45 and 1000 μM nitrate show no evidence of a local maximum. The catalytic currents for these cases increase rapidly on sweeping from 100 to 0 mV and then more slowly on further lowering the applied potential, giving an approximation to a sigmoidal response.

To confirm that the changing shape of the catalytic response reflects intrinsic properties of NarGH, a number of control experiments were performed. Introducing azide, an inhibitor of NarGH (*8*), into these experiments produced voltammograms showing no evidence of a catalytic response, as in Figure 2. Aside from an increase in charging current, these voltammograms were indistinguishable from those obtained when freshly polished electrodes were placed in buffer−electrolyte solution and cycled across the same potential range (not shown). The presence of an enzyme film

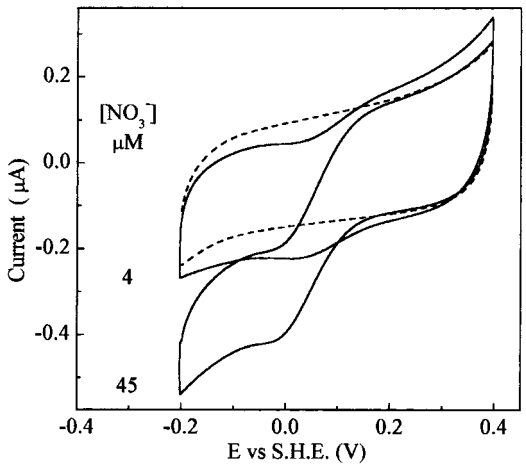

FIGURE 3: Representative cyclic voltammograms from a NarGH film prepared on a gold electrode in 4 and 45 μM nitrate. The broken line illustrates the voltammogram obtained after addition of 100 μM azide to the 45 μM nitrate response. All other conditions are the same as for Figure 2.

was confirmed by the clear catalytic response observed after rinsing the NarGH-coated electrode extensively to remove traces of azide and placing it in a fresh nitrate solution. Substrate depletion at the electrode surface cannot be responsible for the local maximum observed in both sweeps of the catalytic voltammetry at 4 μM nitrate, since this would produce a "peak" in the catalytic response only on sweeping to increasingly negative potentials (*24*, *27*). Product inhibition is also not responsible for the reversible decrease in activity observed in voltammograms obtained at 4 μM nitrate. No changes to the shape of a catalytic response were noted when nitrite was titrated into solutions of various nitrate concentration. A 5-fold excess of nitrite over nitrate was required to achieve significant attenuation (40%) of the catalytic current magnitude.

To exclude the possibility that electrode-dependent phenomena were responsible for the distinctive catalytic voltammetry of NarGH, the behavior of films prepared from the same NarGH stock solution on gold and PGE electrodes were compared. Figure 3 illustrates the clear local maximum in catalytic current observed from a gold electrode coated with NarGH and placed in 4 μM nitrate, which is absent from the response at 45 μM nitrate. The similarity between these voltammograms and those obtained with PGE electrodes was maintained in the responses at 1000 μM nitrate (not shown). Thus, NarGH films on both electrode materials give rise to the same distinctive catalytic voltammetry despite the different nature of the electrode surfaces. Films of NarGH on PGE electrodes were routinely used for these studies since this electrode:film combination gave rise to consistently higher quality catalytic responses; compare Figures 2 and 3.

Having confirmed that the catalytic behavior of NarGH revealed by film voltammetry arises from intrinsic properties of the enzyme film, the current−potential profiles can be attributed to reversible, electrochemically induced modulations of NarGH activity. Catalytic voltammograms for a wide range of nitrate concentrations were examined, and the study was extended to characterize reduction of chlorate, an alternative substrate for the enzyme (*8*). The results presented in Figure 4 represent data collected from several independent

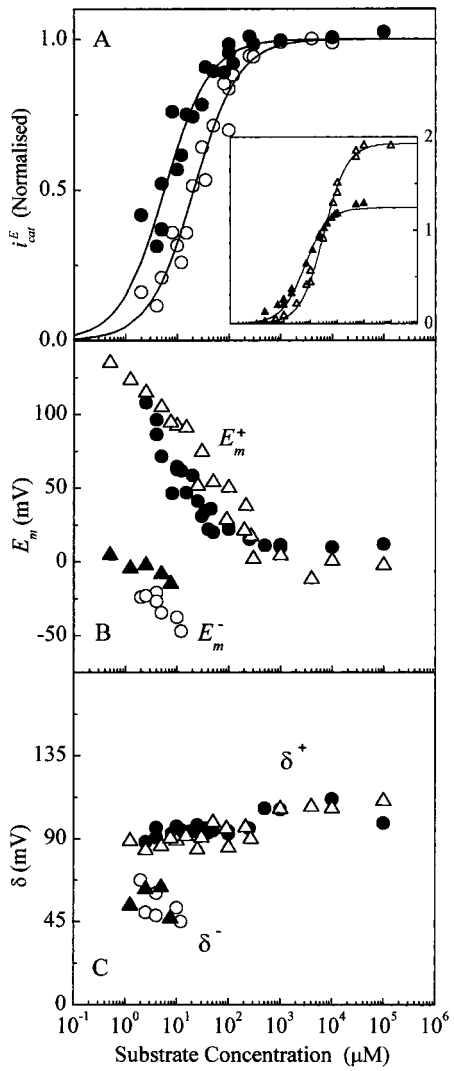

FIGURE 4: Variation of i^E_{cat}, E^+_m, E^-_m, δ^+, and δ^- with nitrate (circles) and chlorate (triangles) concentration for the catalytic voltammetry of NarGH films at pH 6. (A) Variation of i^{+30}_{cat} (closed circles) and i^{-130}_{cat} (open circles) with nitrate concentration. In each case, values of i^E_{cat} are normalized to the maximum response obtained at each potential. Inset: variation of i^{+30}_{cat} (closed triangles) and i^{-130}_{cat} (open triangles) with chlorate concentration normalized to the maximal nitrate response observed at each potential. The solid lines indicate the best fit to the Michaelis−Menten expression in each case; for nitrate, $K^{obs}_M(+30\ mV) = 5.5 \pm 2\ \mu M$ and $K^{obs}_M(-130\ mV) = 21 \pm 5\ \mu M$; for chlorate, $K^{obs}_M(+30\ mV) = 60 \pm 10\ \mu M$ and $K^{obs}_M(-130\ mV) = 310 \pm 40\ \mu M$. (B) Variation of E^+_m with nitrate (solid circles) and chlorate (open triangles) concentration. Variation of E^-_m with nitrate (open circles) and chlorate (solid triangles) concentration. (C) Variation of δ^+ with nitrate (closed circles) and chlorate (open triangles) concentration. Variation of δ^- with nitrate (open circles) and chlorate (closed triangles) concentration. Voltammograms were obtained with NarGH films prepared on PGE electrodes. All other conditions are the same as for Figure 2.

preparations of NarGH, each of which exhibited indistinguishable catalytic protein film voltammetry across the complete range of substrate concentrations investigated. The parameters i^E_{cat}, E_m, and δ represent the magnitude, position, and steepness, respectively, of features in the catalytic response (see below). For both nitrate (circles) and chlorate (triangles), the results reflect a smooth progression of the catalytic waveform from one containing a local maximum at low substrate concentrations to an essentially sigmoidal response as the substrate concentration is raised. Catalytic voltammograms obtained with supporting electrolyte varied from 0 to 1 M Na_2SO_4 in 25 mM Mes (pH 6) confirmed that ionic strength did not influence the results. Similarly, changing the identity of the buffer or its concentration as described in the Experimental Procedures produced no detectable changes in the catalytic voltammetry of NarGH.

A powerful method for examining the position and steepness of features in a catalytic voltammogram is through a plot of the first derivative of catalytic current with respect to applied potential, di/dE. This also highlights visually the differences between various responses as illustrated in Figure 2C where di/dE plots for the voltammograms of Figure 2A are presented. Each catalytic current derivative displays a well-defined positive feature, which reflects the sharp increase in catalytic current observed on first sweeping toward more negative potentials. The potential of maximum amplitude, E^+_m, characterizes the position of this feature in the catalytic response. In Figure 2C, the amplitude of the catalytic current derivatives has been normalized at E^+_m to aid their comparison. For increasing concentrations of nitrate, E^+_m is displaced toward more negative potentials until, at >1 mM nitrate, a limiting value of $E^+_m = +7.5 \pm 5$ mV is approached, as in Figure 4B. Increases of chlorate concentration produce a similar variation of E^+_m, although the absolute values are initially slightly more positive and tend to a limiting potential slightly more negative (-2 ± 5 mV) than those observed with nitrate. Transferring NarGH films between chlorate and nitrate solutions confirmed that subtle differences in the catalytic response from these substrates were reversible and attributable to the identity of the substrate. The half-height width, δ^+, of the positive feature in the catalytic current derivative reflects the steepness of the corresponding component of the catalytic wave, as in Figure 2C. For nitrate and chlorate concentrations below 100 μM, values of δ^+ lie close to 100 mV with a slight increase in δ^+ at higher substrate concentrations. A striking feature of the catalytic current derivatives presented in Figure 2C is the presence of a negative component in the plot corresponding to voltammetry in 4 μM nitrate. With a maximum amplitude at E^-_m, this component of the catalytic current derivative occurs for potentials over which the catalytic current magnitude decreases in response to the application of increasingly negative potentials and hence increased driving force for the reaction catalyzed. Catalytic current derivatives from voltammetry in $\leq 10\ \mu$M nitrate or chlorate clearly displayed this negative component. E^-_m takes increasingly negative values as the substrate concentration approaches 10 μM, as in Figure 4B. When a negative component is present in the catalytic current derivative, its half-height width, δ^-, is consistently smaller than δ^+, reflecting a more rapid (steeper) change in catalytic current when the activity is lowered by applying increasingly negative potentials than when activity is switched on at more positive potentials, as in Figure 2C.

The activity of the enzyme film at each value of applied potential, E, is reflected by the magnitude of the catalytic current, i^E_{cat}, at that potential. Variation of i^E_{cat} with substrate concentration was quantitated at $+30$ and -130 mV to reflect the activities on the high and low potential flanks, respec-

tively, of the catalytic response at lower substrate concentrations, as in Figure 2. As described in the Experimental Procedures, variations of i_{cat}^{E} with substrate concentration were determined in a number of experiments and normalized to the response in a standard solution (typically 1 mM KNO_3 or $KClO_3$, 2 mM neomycin, 25 mM Mes, and 50 mM Na_2SO_4, pH 6, at 25 °C) to account for film to film variation in the magnitude of the response. Results for nitrate are shown in Figure 4A where variation of i_{cat}^{E} relative to the maximal response for that potential, $i_{max}^{E} = 1$, is presented. It is clear that distinct values of K_M^{obs} are observed for the different measurement potentials $K_M^{obs}(+30\text{ mV}) = 5.5 \pm 2\ \mu M$ and $K_M^{obs}(-130\text{ mV}) = 21 \pm 5\ \mu M$ ($i_{max}^{-130}/i_{max}^{+30} = 2.6$). Thus, the local maximum is lost from the catalytic response as current magnitudes at more positive potentials approach a maximum while those at lower potentials continue to increase. A similar pattern of behavior is observed with chlorate as the substrate. The insert to Figure 4 illustrates the variations of i_{cat}^{E} at +30 and −130 mV relative to the corresponding i_{max}^{E} for nitrate reduction from which $K_M^{obs}(+30\text{ mV}) = 60 \pm 10\ \mu M$ and $K_M^{obs}(-130\text{ mV}) = 310 \pm 40\ \mu M$ ($i_{max}^{-130}/i_{max}^{+30} = 3.75$).

Influence of pH on the Nitrate Reductase Activity of NarGH Films. Nitrate concentrations of 4 and 500 μM were chosen to establish the influence of pH on the catalytic voltammetry of NarGH. After recording voltammetry at the pH of interest, NarGH films were transferred to a standard 500 μM nitrate, pH 6 solution where further voltammograms were measured and to which values of i_{cat}^{E} were normalized. Inspection of the absolute currents recorded in the standard solution showed that there were no systematic variations of electroactive film coverage across the pH range of 5−11. The shape, position, and magnitude of the catalytic response were found to be independent of the identity and concentration of the pH buffer in a series of control experiments utilizing phosphate, acetate, citrate, Tris, and Good's buffers and described in the Experimental Procedures. All effects of pH on the voltammetric response were found to be fully reversible during repeated transfers between solutions of distinct pH.

For voltammograms recorded in 500 μM nitrate, the major effect of raising the pH from 5 to 11 is to produce a sigmoidal decrease in i_{cat}^{E}, as in Figure 5. There is no detectable catalytic response above pH 10, and the variation of i_{cat}^{E} with pH is the same at +30 and −130 mV. Negligible changes in E_m^+ or δ^+ were found to accompany the pH-induced changes of signal magnitude. The voltammetric behavior of NarGH is consistent with a pH-induced variation in the concentration of electrocatalytic enzyme in the film. Because the total enzyme population on the electrode surface did not vary across the pH range investigated, changes in the population of electrocatalytic enzyme induced by ionization of the enzyme:substrate complex are being monitored. Voltammetry performed with 100 mM nitrate at pH ≥9.5 confirmed the absence of detectable activity in the more alkaline conditions. The solid line in Figure 5A illustrates how the pH variation of nitrate reductase activity is in good agreement with the expression

$$i_{cat}^{E,pH} = \frac{i_{cat}^{E,pH6} \times 10^{-pH}}{10^{-pH} + 10^{-pK_a}} \qquad (3)$$

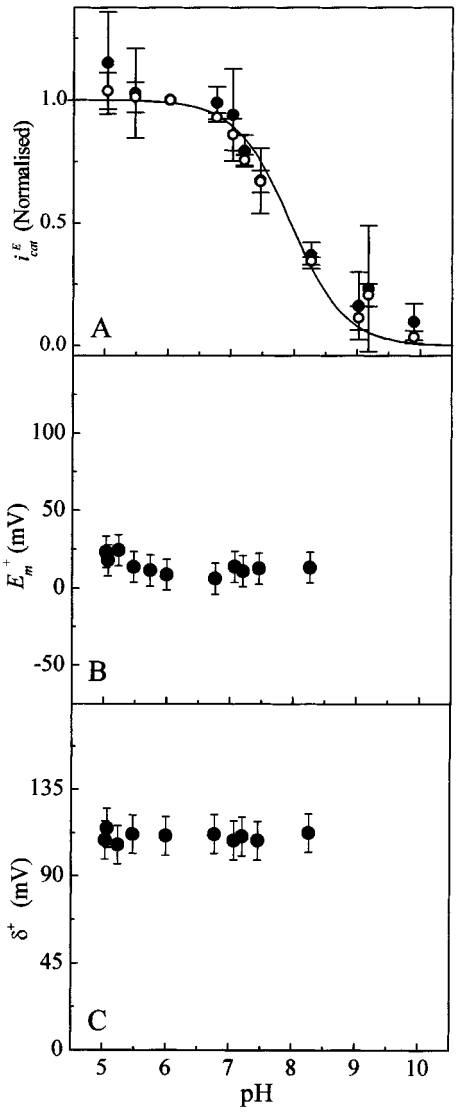

FIGURE 5: pH dependence of i_{cat}^{-130} (open circles) and i_{cat}^{+30} (closed circles), E_m^+, and δ^+ for the catalytic voltammetry of NarGH films in 500 μM nitrate. Values of i_{cat}^{E} were normalized to the response at pH 6.0. The solid line in panel A is the behavior predicted when deprotonation of a single residue with $pK_a = 7.9$ inactivates enzyme under alkaline conditions.

describing activation of an alkaline enzyme form of NarGH by protonation of a single residue with ionization constant K_a where $i^{E,pH}$ is the activity measured at each pH yielding $pK_a = 7.9 \pm 0.2$. Spectrophotometric assays of NarGH nitrate reductase activity produced results ($pK_a = 8.3 \pm 0.3$) in acceptable agreement with those from protein film voltammetry.

At 4 μM nitrate, the catalytic waveforms from NarGH also decreased in magnitude on moving toward more alkaline pH. However, superimposed on this behavior, significant changes in the shape of the waveform were observed with the local maximum most pronounced between pH 6.8 and pH 7.5. This is illustrated in Figure 6 by the forward sweeps of steady-state voltammograms recorded at pH 5.3, 6, and 6.8. Despite these clear changes in the shape of the waveform, the positions of characteristic features in the catalytic current derivative E_m^+, E_m^-, and $E_\times$ (defined in Figure 2C) show only small variations with pH (see Figure 6).

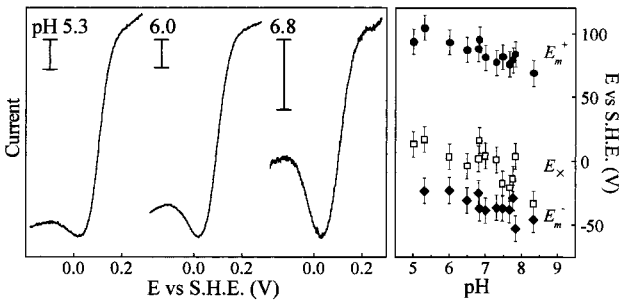

FIGURE 6: Influence of pH on the catalytic voltammetry of NarGH films in 4 μM nitrate. Left panel: forward sweeps of steady-state voltammograms at the indicated pH; the vertical bars indicate 0.5 μA. Right panel: Variation of E_m^+, E_m^-, and $E_\times$ with pH. Voltammograms were recorded in 2 mM neomycin, 50 mM Na_2SO_4, and 10 mM each of acetic acid, Mes, Pipes, Epps, and Ches at the desired pH. All other conditions are the same as for Figure 2.

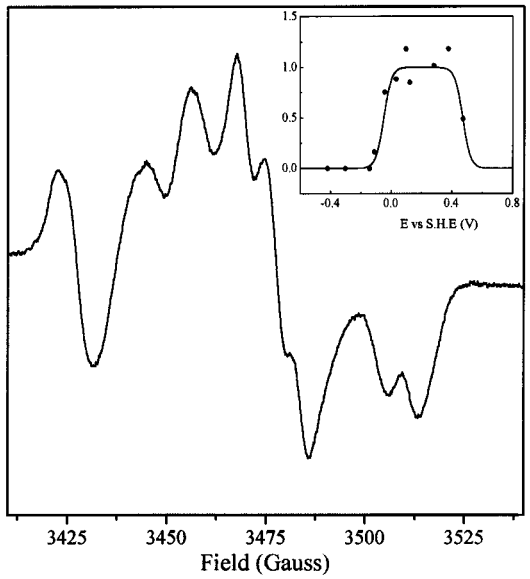

FIGURE 7: Representative EPR spectrum from 80 μM NarGH as isolated measured at 66 K. Inset: variation of signal intensity with potential for the highest field resonance; the line represents the Mo^{5+} signal intensity given by eq 1 with $E_m(Mo^{6+/5+}) = 470$ mV and $E_m(Mo^{5+/4+}) = -50$ mV. Measurement conditions: microwave frequency, 9.668 GHz; microwave power, 13 mW; modulation frequency, 100 kHz; modulation amplitude, 0.2 mT; buffer, 25 mM Mes, pH 6.0.

EPR Characterization and Potentiometric Titration of NarGH at pH 6.0. EPR characterization of NarGH was performed at pH 6.0 where the enzyme exhibited maximal activity. Representative spectra are presented in Figures 7 and 8. At 66 K, the as isolated enzyme exhibits a typical low pH Mo^{5+} rhombic signal split by hyperfine coupling, which when averaged yields apparent g-values of $g_{1,2,3} \sim 2.003, 1.988, 1.969$ (*10*, *18*−*20*). Reduction potentials of the low pH signal giving species were determined by EPR-monitored potentiometric titrations performed under potentiostatic control to avoid the possibility of dithionite or its oxidation products binding at the Mo center. The intensity of the low pH signal was found to be essentially independent of potential across the range +50 to +350 mV. At potentials above and below these limits, the signal intensity decreased as the EPR detectable Mo^{5+} population was transformed into EPR silent Mo^{6+} and Mo^{4+} species, respectively. Reduction potentials of $E_{m,6}(Mo^{6+/5+}) = +470 \pm 20$ mV and $E_{m,6}(Mo^{5+/4+}) = -50 \pm 20$ mV were determined from fitting eq 1 to the variation in amplitude of the highest field resonance with potential; see Figure 7 insert. Close inspection of the spectra provided no evidence of a high pH Mo^{5+} signal. The derivative-shaped resonance located to low field of the Mo^{5+} signal was present to varying extents in NarGH preparations and represents a trace contaminant of uncertain origin.

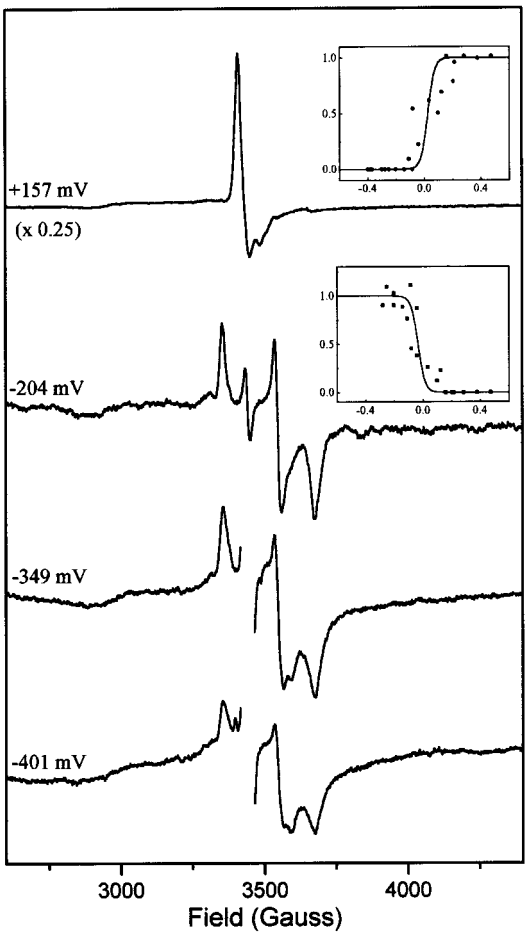

FIGURE 8: Representative EPR spectra measured at 10 K for samples of 40 μM NarGH poised at the indicated potentials. Inset: variation of signal intensity with potential ● for the $[3Fe\text{-}4S]^{1+}$ cluster $g \sim 2.025$ peak where the solid line is a Nernstian fit with $n = 1$ and $E_m = 24$ mV; ■ for a $[4Fe\text{-}4S]^{1+}$ cluster $g \sim 1.833$ trough where the solid line is a Nernstian fit with $n = 1$ and $E_m = -34$ mV. The signal from mediator radicals has been removed from the lower potential spectra for clarity. Measurement conditions: microwave frequency, 9.668 GHz; microwave power, 2 mW; modulation frequency, 100 kHz; modulation amplitude, 0.8 mT; buffer, 25 mM Mes, pH 6.0.

At 10 K, the EPR spectra of NarGH poised at potentials from +470 to −440 mV showed signals typical of [Fe-S] clusters, as in Figure 8. The spectra from samples poised potentiostatically or using dithionite were in acceptable agreement. At potentials above 100 mV, the spectra were essentially indistinguishable and dominated by a signal typical of those arising from $[3Fe\text{-}4S]^{1+}$ clusters with a peak at $g \sim 2.025$. Integration of the $[3Fe\text{-}4S]^{1+}$ signal showed the spin concentration to be in good agreement with that of the fully developed Mo^{5+} signal (1 ± 0.2 spin per molecule). At potentials below 100 mV, the intensity of the $[3Fe\text{-}4S]^{1+}$ signal decreased, and a rhombic signal typical of $[4Fe\text{-}4S]^{1+}$ clusters developed with $g_{1,2,3} \sim 2.062, 1.951$, and 1.883. The $[4Fe\text{-}4S]^{1+}$ signal is maximally developed between −150 and

−230 mV where integration yields a spin concentration in good agreement with that of the fully developed $[3Fe\text{-}4S]^{1+}$ signal (1 ± 0.1 spin equivalents). Reduction potentials for the $[3Fe\text{-}4S]^{1+/0}$ couple and highest potential $[4Fe\text{-}4S]^{2+/1+}$ couple were determined from the amplitude of $g \sim 2.02$ peak and $g \sim 1.883$ trough, respectively. In each case, variation of signal intensity with potential was in acceptable agreement with that anticipated for an $n = 1$ process, yielding $E_{m,6}([3Fe\text{-}4S]^{1+/0}) = 24 \pm 20$ mV and $E_{m,6}([4Fe\text{-}4S]^{2+/1+}) = -34 \pm 20$ mV; see Figure 8 inserts. Lowering the potential below −230 mV produced further changes in the EPR spectrum. Broadening of the existing resonances was accompanied by the appearance of a new resonance at $g \sim 1.923$, consistent with the formation of a second $[4Fe\text{-}4S]^{1+}$ center. Finally, at potentials below ca. −350 mV, formation of a third $[4Fe\text{-}4S]^{1+}$ cluster is suggested by the loss of considerable signal intensity and accompanying broadening of all spectral features as anticipated when coupling of multiple $[4Fe\text{-}4S]^{1+}$ clusters occurs. Because of the complex nature of the signals arising from $[4Fe\text{-}4S]^{1+}$ clusters experiencing weak intercluster interactions and the uncertainty in quantitation of the mediator radical signal, we were unable to determine reduction potentials for the lower potential $[4Fe\text{-}4S]^{1+}$ clusters.

DISCUSSION

Protein film voltammetry provides a powerful tool for studying the catalytic performance of redox enzymes. This is elegantly demonstrated by the catalytic current−potential profiles arising from films of *P. pantotrophus* NarGH, which provide a novel fingerprint of enzyme behavior during substrate reduction. Direct and apparently facile exchange of electrons occurs between NarGH and various electrode materials, and simply by transferring the films between solutions of distinct composition, it has been possible to assess enzyme performance rapidly and with great sensitivity across a wide range of conditions. The overall catalytic behavior of the films is in good agreement with that observed in spectrophotometric assays of NarGH. However, by resolving catalytic activity in the potential domain, a complex pattern of reversible modulations of activity has been revealed. These modulations reflect the consequences of redox events within the enzyme, and distinct behavior is observed dependent on whether catalysis is substrate (nitrate or chlorate) or enzyme limited.

A small but growing number of redox enzymes have been investigated by protein film voltammetry, and the behavior described here for NarGH adds to the variety of responses that have been observed (for example, see refs *25* and *26*). For each enzyme, the question of the origin of the response at a molecular level arises and becomes particularly intriguing when complex modulations of activity such as those exhibited by NarGH are observed. For the simplest case of an enzyme containing a single redox center that is associated with the site of substrate reduction, protein film voltammetry is predicted to yield a sigmoidal catalytic response (*26*). Lowering the electrode potential leads to an increase in the population of reduced and hence catalytically active enzyme on the electrode surface, and the catalytic current increases in a Nernstian manner to approach a limiting, potential independent value. The catalytic currents from NarGH start to increase as the potential is initially lowered. However, for the lower nitrate and chlorate concentrations investigated here, there follows a sigmoidal decrease of the current magnitude to approach a value, which in the first approximation is independent of further lowering of the applied potential. On returning to more positive potentials, the same dependence of NarGH activity on potential is observed, and the entire sequence of modulation is reproduced during repeated potential cycling. The reproducibility of these observations, for different electrode materials and several preparations of NarGH, illustrates how, at these lower substrate concentrations, catalysis at a higher electrode potential and hence with a lower driving force for substrate reduction can occur at a rate in excess of that which can be achieved on application of a higher driving force. Under these conditions, NarGH catalyzes reduction of a single substrate by two kinetically distinct routes distinguished through their specificity constants, k_{cat}^{obs}/K_M^{obs}, and linked reversibly by an electrochemical event. As the substrate concentration increases, the catalytic voltammetry takes an increasingly sigmoidal form, and under conditions of enzyme-limited turnover, the voltammetric response appears to be dominated by substrate reduction through one catalytic pathway.

The similarity of the catalytic voltammetry observed during reduction of the stereochemically distinct substrates nitrate (planar) and chlorate (pyramidal) indicates that the electrochemical modulations of NarGH activity occur independently of substrate-specific interactions within the active site. In the absence of reduction potentials for the NarGH film (*24*), the solution reduction potentials of NarGH defined in this study provide a number of candidates for centers whose electrochemical properties could contribute defining features to the catalytic voltammetry: the Mo-bis-MGD center, the $[3Fe\text{-}4S]^{1+/0}$ cluster with $E_{m,6}$ +24 mV, and the $[4Fe\text{-}4S]^{2+/1+}$ cluster with $E_{m,6}$ −34 mV. However, correlating features in the voltammetry to redox events in the enzyme on the basis of equilibrium reduction potentials is complicated by the substrate concentration dependence of the potential of these features, as in Figure 4. We therefore considered a number of descriptions of enzyme behavior in a first step toward explaining the voltammetry exhibited by NarGH films. As discussed below, two models with distinct mechanistic origins have been found that are able to account for the experimental observations.

A minimal catalytic cycle for active-site chemistry of NarGH was presented in Scheme 1. This cycle has been expanded in Scheme 2 to include sequential one-electron reduction of the Mo center from the 6+ to the 4+ oxidation states and specifies Mo^{5+} in the reductive half cycle. For simplicity, movement of protons, oxo transfer, and water release (necessary for a complete description of the reaction being catalyzed) have been omitted, and the substrate, S, may be nitrate or chlorate. As illustrated in Scheme 2, a simple mechanism by which kinetically distinct pathways can lead to Mo^{4+}:S and hence product formation is available if substrate can associate with the enzyme in its Mo^{5+} and Mo^{4+} oxidation states. The relative rates of substrate and electron addition to Mo^{5+} will determine the predominant route for progression through the catalytic cycle. Whether electrons are delivered to the active site of NarGH in an intermolecular (direct from the electrode) or intramolecular (relayed via the [Fe-S] clusters) process, we anticipate that

Scheme 2: Catalytic Cycle Describing Two-Electron Reduction of a Substrate, S, to Product, P, at a Mo Center Capable of Binding Substrate in the Mo^{5+} and Mo^{4+} Oxidation States[a]

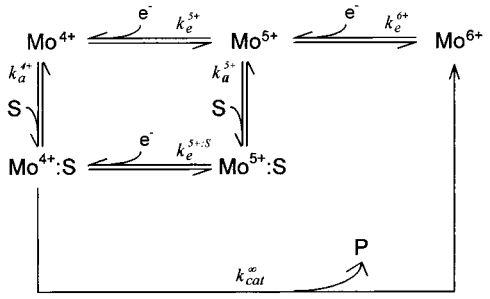

[a] For simplicity, movement of protons, oxo-groups, and water associated with active-site chemistry have been omitted, and only the rate constants for forward progression through the catalytic cycle are indicated. Values for k_a^{y+}, k_{cat}^{∞}, $k_e^{5+:S}$, and $E_m(Mo^{5+/4+}:S)$ are likely to be substrate specific.

the rate of electron addition to Mo^{5+} will increase as the electrode potential is lowered (*24*) and that the voltammograms at low substrate concentrations will show a local maximum if catalysis via Mo^{4+} proceeds with a lower specificity constant than catalysis via Mo^{5+}:S. Kinetic distinction between the two catalytic pathways of Scheme 2 will be lost as substrate concentrations are increased and the rate of catalysis becomes enzyme limited. Under these conditions, a sigmoidal voltammetric response will be observed. Although incorporation of nitrate into the Mo ion's coordination sphere is not a requirement of Scheme 2, if such chemistry does account for the behavior of NarGH, then it is unlikely to occur with the Mo center as Mo^{6+}═O. Thus, although association of nitrate with NarGH in any two of the oxidation states of Scheme 2 can be rationalized as described above to account for the observed voltammetry, the form as written is preferred.

As a more rigorous test of the ability of Scheme 2 to account for the catalytic behavior of NarGH during nitrate reduction, a steady-state analysis was performed as described in the Appendix. Such an approach will provide an accurate description of NarGH voltammetry when rates of electron delivery to the active site do not influence the voltammetric response (*26*). For simplicity, the potential dependence of the rates for electron delivery to the Mo center were described by an expression for interfacial electron transfer (*27*).[4] Values for the parameters describing Scheme 2 were then sought, which reproduced the major features exhibited by NarGH films during nitrate reduction: the appearance of a negative feature in the catalytic current derivative up to ca. 10 μM substrate and displacement of E_m^+ toward more negative potentials as the substrate concentration is raised. The catalytic current derivatives in Figure 9A were generated with C_s equal to 4, 45, and 1000 μM for direct comparison with the experimental results of Figure 2 and illustrate how parameters can be found for which Scheme 2 reproduces the major features in the distinctive voltammetry of NarGH during nitrate reduction, pH 6. The results in Figure 9A were generated with reduction potentials for the Mo center guided by the solution properties of NarGH defined in this study, $k_{cat}^{\infty}(NO_3^-) = 100\ s^{-1}$ estimated as a lower limit for this parameter in our previous voltammetric study (*24*), and other parameters detailed in the figure legend were selected as those that most closely reproduce the experimental observations. Variation of catalytic current magnitude with C_s gave $K_M^{obs}(30\ mV) \approx 4\ \mu M$ and $K_M^{obs}(-130\ mV) \approx 23\ \mu M$. The solution shown is not unique, but with $E_m(Mo^{6+/5+}) \geq E_m(Mo^{5+/4+})$, the general requirement for Scheme 2 to reproduce the behavior of NarGH is that the substrate associates more rapidly and with a lower dissociation constant to Mo^{5+} than Mo^{4+}. While the modeled voltammetry reproduces well the characteristic waveshapes exhibited by NarGH the values of δ are notably larger than those observed

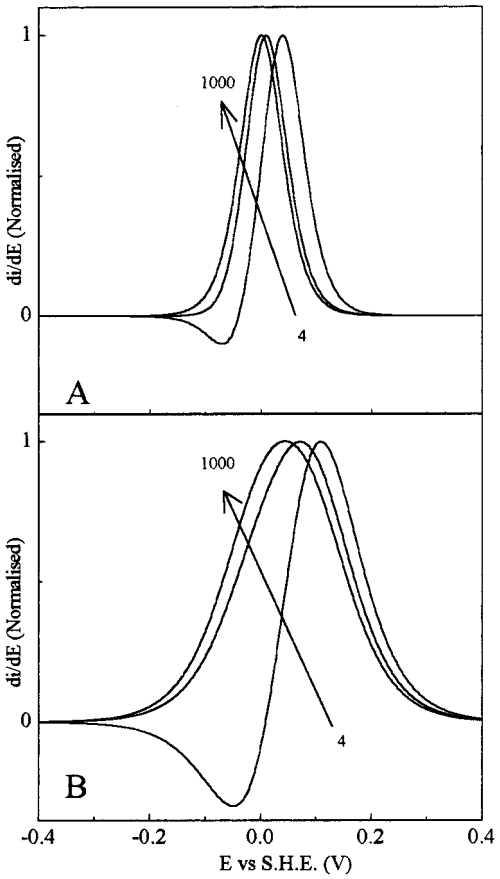

FIGURE 9: Catalytic current derivatives predicted from Scheme 2 in panel A and Scheme 3 in panel B for 4, 45, and 1000 μM substrate concentration; the arrow indicates the direction of increasing substrate concentration. (A) Scheme 2 with $E_m(Mo^{6+/5+}) = 470$ mV; $E_m(Mo^{5+/4+}) = -50$ mV; $E_m(Mo^{5+/4+}:S) = 0$ mV; $k_a^{5+} = 5 \times 10^7\ s^{-1}$; $K_d^{5+} = 1 \times 10^{-6}$ M; $k_a^{4+} = 4 \times 10^7\ s^{-1}$; $K_d^{4+} = 2 \times 10^{-5}$ M; $k_{cat}^{\infty} = 100\ s^{-1}$; and $k_s = 1 \times 10^5\ s^{-1}$ for each electron transfer. (B) Scheme 3 with $E_{cat}^A = 90$ mV; $n_{app}^A = 0.5$; $k_{cat}^A = 40\ s^{-1}$; $K_M^A = 1\ \mu M$; $E_{cat}^B = 100$ mV; $n_{app}^B = 1$; $k_{cat}^B = 100\ s^{-1}$; $K_M^B = 20\ \mu M$; $E_{switch} = 0$ mV; and $n_{switch} = 0.5$.

[4] Electron delivery to the active site of NarGH may occur by relay through a [Fe-S] cluster. When a sufficiently high population of reduced relay center is required to achieve the maximum rate of catalysis for a given substrate concentration, the catalytic voltammetry will reflect the influence of the relay. Such conditions are increasingly likely to be met as the substrate concentration is raised, and the catalytic voltammetry will change from a form dominated by properties of the active site at low substrate concentrations to one increasingly reflecting the influence of the relay center and intramolecular electron transfer as the substrate concentration is raised (*24*). Thus, the behavior of NarGH predicted from Scheme 2 with intramolecular electron transfer via an one-electron relay is also anticipated to take the experimentally observed form.

Scheme 3: Reversible, Redox-Driven Transformation of NarGH between Two Catalytically Competent Forms, A and B, by the Operation of a Redox Switch (oval) with Electron Stoichiometry, *n*

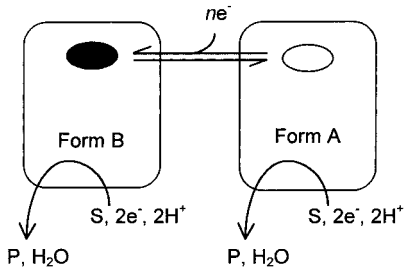

experimentally. This difference between the modeled and the experimental voltammograms becomes less pronounced when the assumption that reduction potentials in the film are equal to those in solution is lifted. When $E_m(Mo^{5+/4+})$ takes slightly more positive values, parameters can be found for which the modeled voltammograms reproduce the experimental voltammograms more fully.

One mechanism through which substrate association with the Mo^{5+} state could facilitate catalysis is through redox-linked modulation of rates of access to and egress from the active site of NarGH. Entrances to the active sites of several Mo-bis-MGD enzymes with homology to NarG possess a surface loop, which in *Rhodobacter capsulatus* DMSO reductase closes to shield substrate-bound active site from solvent and whose movement could be redox linked (*28*−*30*). It is notable that previous EPR spectroscopic studies of *P. denitrificans* and *E. coli* NarGHI have presented evidence to support nitrate association with the Mo^{5+} state of the enzyme in the low pH form (*15*, *18*−*20*). Changes in the number and geometry of ligands in the Mo coordination sphere during redox events may also contribute to a mechanism for kinetic discrimination between the formally Mo^{5+} and Mo^{4+} states of Scheme 2. Such changes are frequently observed in studies of bis(dithiolene)molybdenum(VI) complexes, although the significance of these observations to the catalytic pathways of molybdenum enzymes is unclear at the present time (*31*−*34*).

An alternative means by which a redox event can drive NarGH reversibly between states with different catalytic properties is presented in Scheme 3. Here oxidation or reduction of a center forming a "redox switch" drives the enzyme population toward form A or form B respectively. Each form of the enzyme may exhibit distinct values of k_{cat}^{obs} and K_M^{obs} for a reduction of given substrate. During a voltammetric sweep to increasingly negative potentials NarGH is converted from form A to form B, and the catalytic response changes from one dominated by the properties of form A to one dominated by the properties of form B. By calculating the relative populations of form A and form B at each potential and then summing the catalytic current from each population, the catalytic current−potential profiles from Scheme 3 can be generated. In a first approach to modeling the behavior of NarGH with Scheme 3 we have made the simplifying assumptions that the catalytic current−potential profiles from each enzyme form are sigmoidal and have positions independent of substrate concentration as described in the Appendix. Figure 9B illustrates how the major voltammetric features exhibited by NarGH during nitrate reduction at pH 6 can be reproduced with k_{cat}^{obs}/K_M^{obs} for form B < form A, $E_{switch} = 0$ V, and further parameters as detailed in the figure legend ($K_M^{obs}(30\ mV) = 5\ \mu M$ and $K_M^{obs}(-130\ mV) = 20\ \mu M$). The assumptions described above prevent Scheme 3 from providing a complete description of the voltammetry exhibited by NarGH. Most notably values of δ^+ are always significantly greater than the ca. 100 mV observed experimentally. This feature of the modeled voltammetry will be alleviated if the catalytic response from each enzyme form adopts a position dependent on substrate concentration, and indeed, many simple models for the catalytic voltammetry from enzyme films predict this behavior, even when a simple sigmoidal response is observed (*24*, *26*). Further refinement of Scheme 3 along these lines was considered unwarranted at the present time.

The $[3Fe\text{-}4S]^{1+/0}$ cluster and highest potential $[4Fe\text{-}4S]^{2+/1+}$ cluster have solution reduction potentials similar to that of the redox switch suggested by the modeled voltammograms of Figure 9B. However, it is also possible that the switch has escaped detection by EPR spectroscopy. Alternative candidates for the redox switch are provided by the possibility of NarGH bound quinone, as proposed for the *E. coli* enzyme (*14*) and Mo-bis-MGD based redox chemistry additional to that of the well-characterized $Mo^{6+/5+}$ and $Mo^{5+/4+}$ transitions (*35*, *36*). The mechanism by which a redox switch acting independently of active-site catalytic chemistry could induce distinct activities of form A and form B as presented in Scheme 3 is of considerable interest. Modulation of catalytic activity through conformational changes carried to the active site represents one possibility. This suggestion has also been made in kinetic studies of nitrate reduction by *E. coli* NarGH using benzyl viologen as the electron donor and was proposed to originate from changes in the redox status of [Fe-S] clusters (*37*, *38*). To our knowledge, multiple forms of Mo^{5+} EPR signal indicative of distinct Mo coordination spheres have not been reported during potentiometric titrations of NarGH at pH 6.0. However, such behavior may have gone undetected as it requires an appropriate separation of reduction potentials for significant population of each Mo^{5+} species. Potentiometric titrations of the Mo-bis-MGD containing *P. pantotrophus* NapAB have identified multiple Mo^{5+} signals consistent with the presence of multiple Mo^{5+} states with distinct thiolate coordination (*5*). While the relationship between such changes in coordination sphere and activity is uncertain, it is interesting to note that loss of one or two dithiolene sulfur ligands from the Mo ion on reduction of the switch would generate a state similar to that observed in plant assimilatory nitrate reductases, $Mo^{6+}(O)_2(SR)_{2,3}$ (*17*).

Protein film voltammetry has provided evidence for complex redox-linked modulations of NarGH performance, and Schemes 2 and 3 provide mechanisms that can account for the main voltammetric features exhibited by the enzyme during substrate reduction. The ability of the film voltammetric approach to provide a novel view of enzyme behavior is further illustrated by the response of NarGH films to variation of pH. A decrease in the population of active enzyme by ionization of a residue with $pK_a \approx 7.9$ represents the major pH-induced modulation of activity. However, superimposed on this behavior, the consequences of additional ionization processes are apparent. Increasing the

proton concentration in solutions of 4 μM nitrate causes the catalytic response to change from peak shaped to approximately sigmoidal in a manner that parallels the voltammetric observations made at pH 6 for increasing nitrate concentration. Recently, similar pH-induced changes in the catalytic film voltammetry arising from another Mo-bis-MGD and [Fe-S] cluster containing enzyme were reported (*39*). Variation of catalytic waveshape with pH for the membrane-anchored DMSO reductase from *E. coli* was attributed to a mechanism similar to that shown in Scheme 2 with S as a proton rather than nitrate. It will be of interest to establish whether the catalytic voltammetry of these homologous enzymes arises from a common mechanism.

One final feature of the voltammetry from NarGH deserves further comment. The slow increase in current detectable at most negative potentials of the voltammograms in Figure 2 is not accounted for by our models for which a potential independent current is calculated in this potential region. On extending the voltammetric sweeps to lower potentials, the measured current continues to increase slowly to potentials of at least −800 mV. Our investigations to date suggest that this increase in current originates from substrate reduction by NarGH (not shown). These observations are of interest since, at least in solution, NarGH contains $[4Fe\text{-}4S]^{2+/1+}$ clusters with reduction potentials below −100 mV whose redox status could exert influence over the rate of enzyme turnover in addition to that already discussed.

In summary, the catalytic activity of NarGH when resolved in the potential domain by protein film voltammetry raises many interesting questions about the modulation of enzyme activity by redox events occurring under turnover conditions. Catalysis under substrate-limiting conditions clearly occurs via two pathways with distinct kinetic properties reversibly linked by a redox event. This redox event may be integral to the catalytic cycle of the active site or occur at a center, remote from the description of active-site chemistry, which serves to switch NarGH between two catalytically competent forms. Experiments combining spectroscopic and electrochemical methodologies are now in progress to gain insight into the origin of the distinctive catalytic behavior of NarGH at the molecular level.

ACKNOWLEDGMENT

We thank the Centre for Metalloprotein Spectroscopy and Biology for provision of *P. pantotrophus* cells; David Clarke, Jeremy Thornton, Gareth Butland, and Ann Reilly for assistance with cell growth and protein purification; the John Innes Centre (Norwich) for access to EPR spectroscopy; Dr. Shirley Fairhurst for technical support; Claire Chappell for assistance with the spectrophotometric assays of NarGH activity; and Professor Andrew Thomson for his interest in this work. J.N.B. thanks the Wellcome Trust for a Research Career Development Fellowship.

APPENDIX

Modeling Steady-State Catalytic Voltammetry from Scheme 2. The catalytic current arising from Scheme 2 is given by

$$i_{cat}(E) = -nFA\Gamma_{Mo^{4+}:S}k^{\infty}_{cat} \quad \text{(A1)}$$

where n is the number of electrons required to convert substrate to product, F is the Faraday constant, A is the electrode area, $\Gamma_{Mo^{4+}:S}$ is the concentration of Mo^{4+}:S on the electrode surface at a given potential and substrate concentration, and k^{∞}_{cat} is the rate constant for product formation from Mo^{4+}:S. Under steady-state conditions, $\Gamma_{Mo^{4+}:S}$ can be derived from a consideration of the kinetic and thermodynamic parameters describing electron-transfer and substrate-binding reactions in the catalytic cycle (*25*). For the redox reaction

$$Mo^{y+} + 1e^- \underset{k^{y+}_{-e}}{\overset{k^{y+}_{e}}{\rightleftharpoons}} Mo^{(y-1)+}$$

the surface populations of each species are given by the Nernst equation

$$\theta_{y+} = \frac{\Gamma_{Mo^{y+}}}{\Gamma_{Mo^{(y-1)+}}} = \frac{k^{y+}_{-e}}{k^{y+}_{e}} = \exp\left(\frac{F\{E - E_m(Mo^{y+/(y-1)+})\}}{RT}\right) \quad \text{(A2)}$$

where k^{y+}_{e} and k^{y+}_{-e} are the rate constants for forward and reverse electron transfer, respectively, and all other symbols are as defined in the main text. Reversible binding of substrate to the $y+$ oxidation state of the active site

$$S + Mo^{y+} \underset{k^{y+}_{d}}{\overset{k^{y+}_{a}}{\rightleftharpoons}} M^{y+}:S$$

is described by the dissociation constant, K^{y+}_{d}, given by

$$K^{y+}_{d} = \frac{\Gamma_{Mo^{y+}}C_S}{\Gamma_{Mo^{y+}:S}} = \frac{k^{y+}_{d}}{k^{y+}_{a}} \quad \text{(A3)}$$

where k^{y+}_{a} and k^{y+}_{d} are the rate constants for association and dissociation, respectively. The steady-state differential equations for Scheme 2 are[1,2]

$$\frac{d\Gamma_{Mo^{6+}}}{dt} = k^{\infty}_{cat}\Gamma_{Mo^{4+}:S} + k^{6+}_{-e}\Gamma_{Mo^{5+}} - k^{6+}_{e}\Gamma_{Mo^{6+}} = 0 \quad \text{(A4)}$$

$$\frac{d\Gamma_{Mo^{5+}}}{dt} = k^{6+}_{e}\Gamma_{Mo^{6+}} + k^{5+}_{-e}\Gamma_{Mo^{4+}} + k^{5+}_{d}\Gamma_{Mo^{5+}:S} - \Gamma_{Mo^{5+}}(k^{5+}_{e} + k^{6+}_{-e} + k^{5+}_{a}C_S) = 0 \quad \text{(A5)}$$

$$\frac{d\Gamma_{Mo^{4+}}}{dt} = k^{5+}_{e}\Gamma_{Mo^{5+}} + k^{4+}_{d}\Gamma_{Mo^{4+}:S} - \Gamma_{Mo^{4+}}(k^{5+}_{-e} + k^{4+}_{a}C_s) = 0 \quad \text{(A6)}$$

$$\frac{d\Gamma_{Mo^{5+}:S}}{dt} = k^{5+}_{a}C_S\Gamma_{Mo^{5+}} + k^{5+:S}_{-e}\Gamma_{Mo^{4+}:S} - \Gamma_{Mo^{5+}:S}(k^{5+}_{d} + k^{5+:S}_{e}) = 0 \quad \text{(A7)}$$

$$\frac{d\Gamma_{Mo^{4+}:S}}{dt} = k^{4+}_{a}C_S\Gamma_{Mo^{4+}} + k^{5+:S}_{-e}\Gamma_{Mo^{5+}:S} - \Gamma_{Mo^{4+}:S}(k^{\infty}_{cat} + k^{5+:S}_{-e} + k^{4+}_{d}) = 0 \quad \text{(A8)}$$

from which steady-state surface concentrations for each

species can be obtained as a function of $\Gamma_{Mo^{4+}:S}$

$$\Gamma_{Mo^{4+}} = \left[\Gamma_{Mo^{4+}:S}\left(\frac{K_d^{4+}}{k_a^{5+}} + \frac{k_{cat}^{\infty}}{k_a^{4+}k_a^{5+}} + \frac{K_d^{4+}C_S}{k_e^{5+}} + K_d^{5+}\left\{\frac{K_d^{4+}}{k_e^{5+:S}} + \frac{k_{cat}^{\infty}}{k_a^{4+}k_e^{5+:S}} + \frac{\theta_{5+S}}{k_a^{4+}}\right\}\right)\right] / \left[C_S\left(\frac{\theta_{5+}}{k_a^{4+}} + \frac{C_S}{k_e^{5+}} + \frac{K_d^{5+}}{k_e^{5+:S}} + \frac{1}{k_a^{5+}}\right)\right] \quad \text{(A9)}$$

$$\Gamma_{Mo^{6+}} = \Gamma_{Mo^{4+}S}\left(\frac{K_d^{5+}\theta_{6+}}{C_S}\left\{\frac{k_a^{4+}K_d^{4+}}{k_e^{5+:S}} + \frac{k_{cat}^{\infty}}{k_e^{5+:S}} + \theta_{5+:S}\right\} + \frac{\theta_{6+}}{k_a^{5+}}\left\{\frac{k_a^{4+}K_d^{4+} + k_{cat}^{\infty}}{C_S}\right\} + \frac{k_{cat}^{\infty}}{k_e^{6+}}\right) - \Gamma_{Mo^{4+}}\theta_{6+}k_a^{4+}\left(\frac{K_d^{5+}}{k_e^{5+:S}} + \frac{1}{k_a^{5+}}\right) \quad \text{(A10)}$$

$$\Gamma_{Mo^{5+}} = [\Gamma_{Mo^{4+}:S}(k_{cat}^{\infty}\{k_a^{5+}K_d^{5+} + k_e^{5+:S}\} + k_a^{5+}k_e^{5+:S}K_d^{5+}\theta_{5+:S}) + \Gamma_{Mo^{4+}}(k_e^{5+}\theta_{5+}\{k_a^{5+}K_d^{5+} + k_e^{5+:S}\})] / [k_e^{5+:S}(k_e^{5+} + k_a^{5+}C_S) + k_e^{5+}k_a^{5+}K_d^{5+}] \quad \text{(A11)}$$

$$\Gamma_{Mo^{5+}:S} = \frac{\Gamma_{Mo^{5+}}C_S}{K_d^{5+}}\left(\frac{k_a^{4+}}{k_a^{5+}} + \theta_{5+} + \frac{k_a^{4+}C_S}{k_e^{5+}}\right) - \frac{\Gamma_{Mo^{4+}:S}}{K_d^{5+}}\left(\frac{k_a^{4+}K_d^{4+}}{k_a^{5+}} + \frac{k_a^{4+}K_d^{4+}C_S}{k_e^{5+}} + \frac{k_{cat}^{\infty}}{k_a^{5+}}\right) \quad \text{(A12)}$$

From the mass balance relationship

$$\Gamma_{tot} = \Gamma_{Mo^{6+}} + \Gamma_{Mo^{5+}} + \Gamma_{Mo^{4+}} + \Gamma_{Mo^{5+}:S} + \Gamma_{Mo^{4+}:S} = 1 \quad \text{(A13)}$$

an expression for $\Gamma_{Mo^{4+}:S}$ in terms of the electrode potential and substrate concentration at the electrode surface, C_S, can be obtained. The steady-state current arising from Scheme 2 is then available from substitution of $\Gamma_{Mo^{4+}:S}$ into eq A1. For NarGH, C_S is equated to the substrate concentration in bulk solution since the response at steady state is independent of the rate of electrode rotation. The rate constants describing electron delivery to the active site will be potential dependent whether these are intramolecular or interfacial processes (*24*). For ease of calculation, we assume that electron delivery to the active site is not rate limiting and describe k_e^{y+} by Butler−Volmer expressions for interfacial electron transfer

$$k_e^{y+} = k_s \exp\left(\frac{-0.5F\{E - E_m(Mo^{y+/(y-1)+})\}}{RT}\right) \quad \text{(A14)}$$

where $k_s = k_e^{y+}$ when $E = E_m(Mo^{y+/(y-1)+})$ (*27*).

Certain features of the sets of modeled voltammograms with properties similar to those of NarGH are worth comment. The catalytic current derivatives show displacement of E_m^- to more negative potentials with an increase of C_S, which reflects the need to apply lower potentials before the rate of electron delivery to Mo^{5+} exceeds $k_a^{5+}C_S$, when the latter is increased by an increase of substrate concentrations. It is interesting to note that the catalytic voltammogram from Scheme 2 under enzyme-limiting conditions reflects the reduction potential of the Mo center with substrate-bound $E_m(Mo^{5+/4+}:S)$.

Modeling Catalytic Voltammetry from Scheme 3. The catalytic current−potential profile arising from Scheme 3 will be given by extension of eq A1 to account for contributions to the catalytic current from the distinct Mo^{4+}:S states of form A and form B. At a given potential, the populations of forms A and B, Γ_X, are available from the Nernst equation, given the reduction potential of the switch, E_{switch}, and its apparent electron stoichiometry, n_{switch}:

$$\Gamma_A/\Gamma_B = \exp(n_{switch}F(E - E_{switch})/RT) = \theta_s \quad \text{(A15)}$$

Consideration of appropriate catalytic mechanisms for each of forms A and B would provide a full description of the catalytic current−potential profile through the steady-state approach outlined above. Here, for simplicity, we describe the population of reduced catalytically competent enzyme in each form ($\Gamma_{X^{red}}$) through the Nernst equation, using an apparent reduction potential (E_{cat}^X) and electron stoichiometry (n_{app}^X):

$$\Gamma_{X^{ox}}/\Gamma_{X^{red}} = \exp(n_{app}^X F(E - E_X)/RT) = \theta_X \quad \text{(A16)}$$

Taking into account mass balance

$$\Gamma_{A^{red}} = \frac{\Gamma_A}{(1 + \theta_A)} = \frac{1}{(1 + \theta_A)(1 + \theta_s^{-1})} \quad \text{(A17)}$$

and

$$\Gamma_{B^{red}} = \frac{\Gamma_B}{(1 + \theta_B)} = \frac{1}{(1 + \theta_B)(1 + \theta_s)} \quad \text{(A18)}$$

Assuming that only the reduced state of each form is active and taking no account of variations of apparent reduction potentials induced when substrate binds to the enzyme, the rate of enzyme-catalyzed substrate reduction is then given by the appropriate Michaelis−Menten expression to yield

$$i_{cat}(E) = -nFAC_S\left(\frac{k_{cat}^A\,\Gamma_{A^{red}}}{C_S + K_M^A} + \frac{k_{cat}^B\,\Gamma_{B^{red}}}{C_S + K_M^B}\right) \quad \text{(A19)}$$

REFERENCES

1. Richardson, D. J. (2000) *Microbiology* (*Reading, U.K.*) *146*, 551−571.
2. Berks, B. C., Ferguson, S. J., Moir, J. W. B., and Richardson, D. J. (1995) *Biochim. Biophys. Acta 1232*, 97−173.
3. Berks, B. C., Richardson, D. J., Robinson, C., Reilly, A., Aplin, R. T., and Ferguson, S. J. (1994) *Eur. J. Biochem. 220*, 117−124.
4. Breton, J., Berks, B. C., Reilly, A., Thomson, A. J., Ferguson, S. J., and Richardson, D. J. (1994) *FEBS Lett. 345*, 76−80.
5. Butler, C. S., Charnock, J. M., Bennett, B., Sears, H. J., Reilly, A. J., Ferguson, S. J., Garner, C. D., Lowe, D. J., Thomson, A. J., Berks, B. C., and Richardson, D. J. (1999) *Biochemistry 38*, 9000−9012.
6. Bell, L. C., Richardson, D. J., and Ferguson, S. J. (1990) *FEBS Lett. 265*, 85−87.
7. Parsonage, D., and Ferguson, S. J. (1983) *FEBS Lett. 153*, 108−112.
8. Craske, A., and Ferguson, S. J. (1986) *Eur. J. Biochem. 158*, 429−436.
9. Guigliarelli, B., Magalon, A., Asso, M., Bertrand, P., Frixon, C., Giordano, G., and Blasco, F. (1996) *Biochemistry 35*, 4828−4836.

10. Magalon, A., Asso, M., Guigliarelli, B., Rothery, R. A., Bertrand, P., Giordano, G., and Blasco, F. (1998) *Biochemistry 37*, 7363−7370.
11. Rothery, R. A., Blasco, F., Magalon, A., Asso, M., and Weiner, J. H. (1999) *Biochemistry 38*, 12747−12757.
12. Hensel, M., Hinsley, A. P., Nikolaus, T., Sawers, G., and Berks, B. C. (1999) *Mol. Microbiol. 32*, 275−287.
13. Berks, B. C., Page, M. D., Richardson, D. J., Reilly, A., Cavill, A., Outen, F., and Ferguson, S. J. (1995) *Mol. Microbiol. 15*, 319−331.
14. Magalon, A., Rothery, R. A., Giordano, G., Blasco, F., and Weiner, J. H. (1997) *J. Bacteriol. 179*, 5037−5045.
15. George, G. N., Turner, N. A., Bray, R. C., Morpeth, F. F., Boxer, D. H., and Cramer, S. P. (1989) *Biochem. J. 259*, 693−700.
16. Anderson, L. J., Charnock, J. M., Garner, C. D., Butt, J. N., and Richardson, D. J., unpublished observations.
17. Hille, R. (1996) *Chem. Rev. 96*, 2757−2816.
18. Vincent, S. P., and Bray, R. C. (1978) *Biochem. J. 171*, 639−647.
19. George, G. N., Bray, R. C., Morpeth, F. F., and Boxer, D. H. (1985) *Biochem. J. 227*, 925−931.
20. Turner, N., Ballard, A. L., Bray, R. C., and Feguson, S. (1988) *Biochem. J. 252*, 925−926.
21. Bennett, B., Benson, N., McEwan, A. G., and Bray, R. C. (1994) *Eur. J. Biochem. 225*, 321−331.
22. Rothery, R. A., Magalon, A., Giordano, G., Guigliarelli, B., Blasco, F., and Weiner, J. H. (1998) *J. Biol. Chem.* 273, 7462−7469.
23. Ballard, A. L., and Ferguson, S. J. (1988) *Eur. J. Biochem. 174*, 207−212.
24. Anderson, L. J., Richardson, D. J., and Butt, J. N. (2000) *Faraday Discuss. 116*, 155−169.
25. Armstrong, F. A., Heering, H. A., and Hirst, J. (1997) *Chem. Soc. Rev. 26*, 169−179.
26. Heering, H. A., Hirst, J., and Armstrong, F. A. (1998) *J. Phys. Chem. B 102*, 6889−6902.
27. Bard, A. J., and Faulkner, L. F. (1980) *Electrochemical Methods, Fundamentals and Applications*, John Wiley & Sons, Inc., New York.
28. Czjzek, M., Dos Santos, J.-P., Pommier, J., Giordano, G., Méjean, V., and Haser, R. (1998) *J. Mol. Biol. 284*, 435−447.
29. Dias, J. M., Than, M. E., Humm, A., Huber, R., Bourenkov, G. P., Bartunik, H. D., Bursakov, S., Calvete, J., Caldeira, J., Carneiro, C., Moura, J. J. G., Moura, I., and Romão, M. J. (1999) *Structure 7*, 65−79.
30. McAlpine, A. S., McEwan, A. G., and Bailey, S. (1998) *J. Mol. Biol. 275*, 613−623.
31. Donahue, J. P., Goldsmith, C. R., Nadiminti, U., and Holm, R. H. (1998) *J. Am. Chem. Soc. 120*, 12869−12881.
32. Musgrave, K. B., Donahue, J. P., Lorber, C., Holm, R. H, Hedman, B., and Hodgson, K. O. (1999) *J. Am. Chem. Soc. 121*, 10297−10307.
33. Inscore, F. E., McNaughton, R., Westcott, B. L., Helton, M. E., Jones, R., Dhawan, I. K., Enemark, J. H., and Kirk, M. L. (1999) *Inorg. Chem. 38*, 1401−1410.
34. Oku, H., Ueyama, N., and Nakamura, A. (1995) *Inorg. Chem. 34*, 3667−3676.
35. Luykx, D. M. A. M., Duine, J. A., and de Vries, S. (1998) *Biochemistry 37*, 11366−11375.
36. George, G. N., Costa, C., Moura, J. J. G., and Moura, I. (1999) *J. Am. Chem. Soc. 121*, 2625−2626.
37. Buc, J., Santini, C.-L., Blasco, F., Giordani, R., Cárdenas, M. L., Chippaux, M., Cornish-Bowden, A., and Giordano, G. (1995) *Eur. J. Biochem. 234*, 766−772.
38. Bennett, B., and Bray, R. C. (1993) *Biochem. Soc. Trans. 22*, 78S.
39. Heffron, K., Léger, C., Rothery, R. A., Weiner, J. H., and Armstrong, F. A. (2001) *Biochemistry 40*, 3117−3126.

BI002706B